ARTICLE

Wiley

H₂O time histories in the H₂-NO₂ system for validation of NOx hydrocarbon kinetics mechanisms

Clayton R. Mulvihill



Olivier Mathieu | Eric L. Petersen

J. Mike Walker '66 Department of Mechanical Engineering, Texas A&M University, College Station, Texas

Correspondence

Clayton R. Mulvihill, J. Mike Walker '66 Department of Mechanical Engineering, Texas A&M University, College Station, TX 77843. Email: cmulvihill@tamu.edu

Funding information

National Science Foundation, Grant/Award Number: CBET-1706825

Abstract

The development and refinement of NOx chemical kinetic mechanisms have been instrumental in understanding and reducing NOx formation. However, relatively little work has been performed with NOx species as the oxidizer, and such experiments can provide unique insights into NOx kinetics. Furthermore, speciation data can often provide useful information that complements global measurements such as ignition delay times in facilitating mechanism refinement. To provide such speciation data in the H₂-NO₂ system, H₂O measurements were performed using a fixed-wavelength, direct absorption laser diagnostic near 1.39 µm behind reflected shock waves in fuel-lean, near-stoichiometric, and fuel-rich mixtures of H₂ and NO₂ highly diluted in argon. Experiments were performed between 917 and 1782 K near atmospheric pressure. The H_2O profiles obtained herein are markedly different from those using O_2 as the oxidizer obtained in a previous study. The GRI 3.0 mechanism was found to greatly underestimate the H₂O formation, whereas two modern mechanisms were found to predict the H₂O formation quite accurately except at colder temperatures for fuel-rich conditions. Explanations for the differences between these mechanisms are given and discussed, with the conclusion that older mechanisms such as GRI 3.0 should not be used to model hydrocarbon/NOx combustion chemistry as they are lacking several key reactions and species, namely NO₃ and HONO. The discrepancy between models and data at lower temperatures could not be reconciled even when modifying two of the most-sensitive reaction rates. To the best of the authors' knowledge, this study presents the first shock-tube speciation study in the H₂-NO₂ system.

KEYWORDS

hydrogen, laser absorption, nitrogen dioxide, shock tube

1 | INTRODUCTION

NOx pollutants (NO, NO2, and N2O) are regulated byproducts of hydrocarbon combustion; thus, their mitigation is a matter of key concern in gas turbine design and operation. One technique often employed in practical devices to reduce NOx formation is exhaust gas recirculation (EGR). In EGR, a portion of the exhaust gases is reintroduced to the inlet of the combustor, thereby lowering the temperature and ultimately reducing the level of NOx produced.¹ However, these recirculated gases unavoidably contain some level of NOx, which can have a marked impact on the fuel combustion. In light of this impact, numerous studies have investigated the effects of NOx on various fuel systems. For example, the work by Chan et al² and references therein comprise a comprehensive overview of the studies on NOx-sensitized CH₄.

Of interest to the present work is the effect of NOx (specifically NO₂) on H₂ combustion chemistry. The H₂ mechanism

© 2019 Wiley Periodicals, Inc. 669 Int J Chem Kinet. 2019;51:669-678. wileyonlinelibrary.com/journal/kin

is critical to understanding any hydrocarbon combustion system as this mechanism contains many of the key elementary reaction of important radicals (O, H, OH). Furthermore, H_2 is formed in varying quantities during combustion of higher-order hydrocarbons. For these reasons, the H_2 - O_2 system is the most fundamental combustion system and has accordingly been the topic of a vast number of experimental and theoretical studies.³

The sensitization of H₂-O₂ combustion by NO₂ addition has been studied numerous times in shock tubes,⁴ flow reactors,⁵ and jet-stirred reactors,⁶ among others. However, in each of these cases, the primary combustion system was H₂-O₂, with only trace amounts of NO₂ added to the mixtures. Contrastingly, the H₂-NO₂ system has received a small number of studies, most of which were at relatively low temperatures. The early works of Ashmore and Levitt^{7–9} provided NO₂ time histories using broadband absorption between 445 and 500 nm. NO2 profiles were measured in the presence of varying amounts of H2 and also NO8,9 between 684 and 843 K. Rosser and Wise 10 used absorption of NO_2 to measure time histories in mixtures of H₂-NO₂ between 600 and 700 K in a quartz static reactor. Sawyer and Glassman¹¹ performed flow reactor experiments in H₂-NO₂ mixtures between 850 and 1110 K, ultimately extracting several reaction rate coefficients from their data using temperature profiles measured with a thermocouple inserted into the flow. Park et al¹² performed H2-NO2 oxidation studies in a quartz static reactor between 602 and 954 K by measuring NO, NO2, CO, and CO₂ time histories. Park et al used their results to propose updated rate constants for the reactions $H_2 + NO_2 \rightleftharpoons HONO$ + H (R5) and $2NO_2 \rightleftharpoons 2NO + O_2$. Mueller et al¹³ performed flow reactor studies of H₂-NO₂ mixtures primarily near 830 K to measure the rate of (R5) at a single temperature using time histories of NO, NO2, and H2O. Interestingly, Mueller et al focused primarily on their NO2 and NO profiles and did not address the single H₂O time history they provided.

The primary goal of this paper is to provide new H₂O time histories in the H₂-NO₂ system at higher temperatures (917-1662 K) near 1 atm at three different equivalence ratios in high levels of Ar dilution. These unique data will help to ameliorate the lack of high-temperature data in the H₂-NO₂ system and will permit further testing and validation of chemical kinetic mechanisms that can be used to improve predictions for both the design and operation of low-NOx processes. Secondarily, this paper seeks to point out the key reaction pathways at these higher temperatures and to illustrate potential areas for future refinement. Presented herein are descriptions of the shock-tube facility and H₂O laser diagnostic, followed by the experimental results alongside predictions from several chemical kinetic mechanisms. Finally, an analysis of the reaction pathways and reaction rate sensitivities is given.

2 | EXPERIMENTAL SETUP

2.1 | Shock tube

Experiments were performed in a stainless steel shock tube. The driver side has a length of 3.25 m and an inner diameter of 7.62 cm, while the driven side has a length of 7.88 m and an inner diameter of 16.24 cm. A mechanical pump and a turbomolecular pump were used to vacuum down the driven side to $\sim 10^{-5}$ Torr before each experiment. Polycarbonate diaphragms of thickness 0.254 mm were burst using He as the driver gas. Five fast-response, piezoelectric pressure transducers monitored the passage of the incident shock wave along the last 2 m of the shock tube. The four shock velocities from this measurement were extrapolated to obtain the incident shock wave velocity (v_s) at the endwall of the shock tube, which was then used to calculate the temperature (T_5) and pressure (P_5) behind the reflected shock wave. Uncertainties in T_5 and P_5 are estimated at 0.8% and 1.0%, respectively, arising primarily from uncertainty in v_s . Test times, defined as the interval between the arrival of the reflected shock wave and the expansion wave from the driver side at the measurement location (1.6 cm from the endwall), were typically \sim 3.0 ms for the conditions herein.

Mixtures were prepared using the partial pressure method in a stainless steel mixing tank using capacitance manometers with ranges of 0-10 Torr, 0-1000 Torr (both Baratron MKS 626) and 0-13000 Torr (Setra 225). The Ar and H₂ were supplied by Praxair at 99.999% purity. The NO₂ (99.5% purity) was supplied by Praxair as a mixture of 1.02% NO₂ ($\pm 2\%$) in balance Ar. The tank was vacuumed down to $\sim 10^{-6}$ Torr prior to mixture preparation, and mixtures were allowed to mix for at least 1 h before performing experiments.

2.2 | Laser diagnostic

A tunable diode laser was employed to generate light near 1.39 μ m with a linewidth of ~1 MHz. The laser was tuned to 1388.140 nm to access the $5_{5,1} \leftarrow 5_{5,0}$ transition in the $v_1 + v_3$ fundamental band of H₂O. A Burleigh WA-1000 wavemeter monitored the laser wavelength of a small portion (~10%) of the beam. Two InGaAs detectors with 150-kHz bandwidths monitored the incident (I_0) and transmitted (I_t) beam intensities, with the transmitted beam having been directed through two sapphire window ports located 1.6 cm from the endwall of the shock tube. Both detectors were fitted with bandpass filters (center 1384 nm, full width 10 nm) to mitigate broadband emission. In keeping with the detector bandwidth, all laser profiles were postprocessed using a digital filter with a 150-kHz cutoff frequency. The detectors and optics were enclosed and purged with N₂ to keep the relative humidity below 0.1%.

H₂O concentrations were calculated using the measured transmission profiles in conjunction with the Beer-Lambert

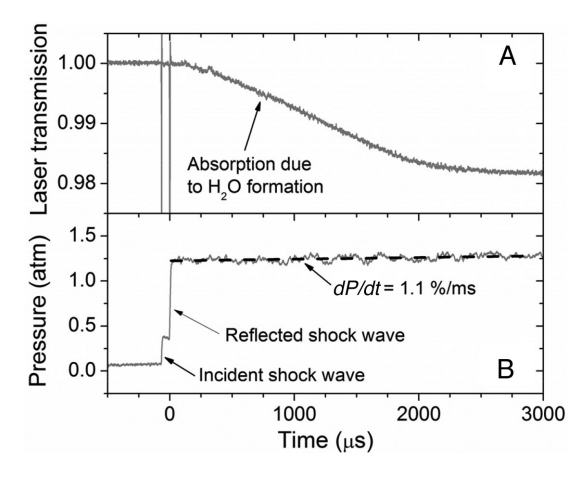


FIGURE 1 Representative (A) laser transmission and (B) pressure time histories measured 1.6 cm from the endwall of the shock tube. The mixture is 0.168% NO₂/1.778% H₂/balance Ar, and the calculated T_5 and P_5 are 1050 K and 1.23 atm

law, $I_t/I_0 = \exp(-k_v P L X_{\rm abs})$, where k_v is the absorption coefficient, P is the pressure, L is the path length (16.24 cm), and $X_{\rm abs}$ is the mole fraction of the absorbing species. The pressure P was monitored using the last piezoelectric pressure transducer located in the same axial plane as the sapphire windows. The absorption coefficient k_v was calculated using known line strength and line shape information as described in Mulvihill et al. ¹⁴ Sample laser transmission and pressure time histories are shown in Figure 1. The two sharp spikes in the laser signal are manifestations of the steep density gradients associated with shock waves and do not signify any physical H_2O formation. The second spike coincides with the arrival of the reflected shock wave and serves as a useful indication of time zero.

The pressure trace in Figure 1 exhibits a nonideal pressure rise (dP/dt) that slightly alters the nominal T_5 and P_5 after the arrival of the reflected shock wave. Additionally, the exothermicity of the mixtures used herein caused a temperature rise (typically ~40 K by the end of the test time). The mechanism of Zhang et al¹⁵ was used to estimate the temperature rise from exothermicity, and both the dP/dt effects and the exothermicity were accounted for by correcting k_{ν} as a function of time. For more information on these corrections, see Mulvihill et al.¹⁴ The dP/dt value for each experiment is provided in the Supporting Information (Tables S1-S3). Incorporating uncertainty introduced by dP/dt, the overall uncertainty in the measured H₂O mole fraction is estimated to be $\pm 5.7\%$.¹⁴

2.3 | LED sensor for mixture validation

In preliminary tests, it was observed that the fuel-rich and near-stoichiometric mixtures (where NO_2 is the limiting reactant involved in H_2O formation) yielded a significantly lower H_2O concentration than expected. On the other hand, the fuel-lean mixture (where H_2 is the limiting reactant) yielded pre-

cisely the amount of $\rm H_2O$ expected. These observations led to the realization that a smaller quantity of $\rm NO_2$ was being added to the mixtures than intended, which can be explained by the well-known dimerization of $\rm NO_2$ to $\rm N_2O_4$. For example, chemical equilibrium calculations reveal that 1.02% $\rm NO_2$ in balance Ar at 298 K and 1300 Torr (typical mixing tank conditions) stabilizes to 9% $\rm N_2O_4$ and 91% $\rm NO_2$. Although the $\rm N_2O_4$ will disappear (< 0.1% of the $\rm NO_2$ concentration) at typical driven-side fill conditions (298 K, 50 Torr) prior to the incident shock wave arrival, $\rm N_2O_4$ in the mixing tank can still present issues by changing the number of moles present in the mixture, therefore introducing error into the partial pressure method of mixture preparation.

To overcome this issue, a simple light-emitting diode (LED) based NO_2 diagnostic was developed. Light from a blue LED was directed through a series of focusing optics and through an aluminum absorption cell with a path length of 11.74 cm before terminating on an InGaAs detector. The light was filtered with a bandpass filter (center 459 nm, full width 5 nm). The NO_2 absorption coefficient measured by Schneider et al¹⁶ was integrated over the filtered spectrum to yield a value of 10.59 cm⁻¹ atm⁻¹. Calibration tests performed with a bottle of known NO_2/Ar concentration yielded excellent agreement with predictions using this absorption coefficient value. The bottle of known NO_2 concentration was prepared by Praxair using the gravimetric filling method, which is insensitive to NO_2 dimerization. The estimated uncertainty of the LED method is $\pm 4\%$ of the measurement value.

The LED diagnostic was used in conjunction with the aluminum absorption cell to measure the NO2 concentration of the fuel-lean mixture, for which the plateau value of H₂O reveals no information about the NO₂ content of the mixture. For the fuel-rich and near-stoichiometric mixtures, the plateau value of H_2O was used to infer the amount of NO_2 present in the initial mixture. Note that this inference was made with the assumption that only one of the O atoms from the NO₂ breaks off to form H₂O; chemical kinetic calculations with a number of mechanisms revealed that the second O atom only begins to form H₂O after an excessive period of time (on the order of minutes for the temperatures investigated in this study). To ascertain the level of agreement between the LED diagnostic and the plateau H₂O methods, a test was performed using both methods. Shown in Figure 2 are a H₂O time history and the calculated theoretical plateau of H₂O using the LED method. The two methods agree within their respective uncertainties, validating the use of both methods in verifying the amount of NO_2 in the initial mixture for each experiment.

The three mixtures used in the present study are listed in Table 1 along with the corresponding T_5 range. The H_2 and Ar concentrations were measured using the typical partial pressure method, whereas the NO_2 concentrations were measured using either the LED (for Mix 1) or plateau H_2O (for Mix 2 and Mix 3) method. The estimated relative uncertainty for

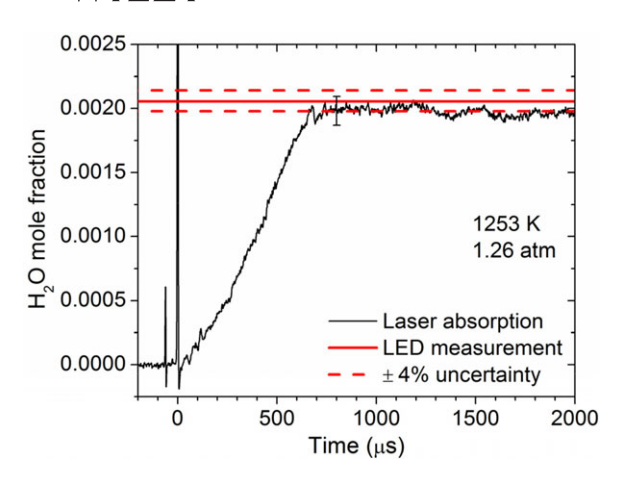


FIGURE 2 Comparison of the plateau $\rm H_2O$ and LED diagnostic methods for measuring the amount of $\rm NO_2$ present in the mixture. The mixture is 0.2055% $\rm NO_2/1.778\%~H_2/Ar$ [Color figure can be viewed at wileyonlinelibrary.com]

TABLE 1 Description of mixtures used in the present study and the corresponding ranges of T_5 investigated

Mixture	% H ₂	% NO ₂	% Ar	φ	T_5 (K)
Mix 1	0.222	0.375^{a}	99.403	0.30	1313-1782
Mix 2	0.444	0.178^{b}	99.378	1.25	1087-1662
Mix 3	1.778	0.168^{b}	98.054	5.29	917-1520

^aMeasured using LED diagnostic.

the NO_2 mole fraction is $\pm 4\%$, whereas for H_2 and Ar it is less than 1%. The equivalence ratio φ was calculated assuming that both O atoms in NO_2 eventually form H_2O . However, only one O atom reacts in the timescales of the present experiments, and one may therefore consider the effective φ as being twice that reported in Table 1. The mixtures tested herein, while highly dilute, are insensitive to impurity effects for the same reasons laid out by Mulvihill et al¹⁴; this was confirmed via kinetic calculations with trace H impurities.

3 | RESULTS

Figure 3 shows 12 H_2O profiles measured in the three mixtures of Table 1; five additional H_2O profiles are provided in the Supporting Information (Figures S1-S5). Although variations due to temperature and φ are evident, each profile exhibits similar features: following the passage of the reflected shock wave, H_2O formation immediately begins and is followed by eventual achievement of a partial equilibrium plateau of H_2O , except for the coldest experiments.

Also shown in each panel of Figure 3 are the modeled H₂O profiles predicted by four separate chemical kinetic mechanisms: those of Zhang et al.¹⁵, Mathieu et al.¹⁷ GRI 3.0,¹⁸ and Glarborg et al.¹⁹ The mechanism predictions were

calculated within the Chemkin software package via the closed homogenous batch reactor using the constant-energy, constant-volume assumption. For highly dilute mixtures such as these, the constant-pressure assumption yields nearly identical predictions. All model predictions were performed using the volume as a function of time method, 20 which accounts for slight, nonideal dP/dt effects, and with the average dP/dtacross all experiments herein of 2.4%/ms, although the dP/dt correction to k_y used the dP/dt value for each individual experiment. The Zhang et al mechanism was modified slightly to incorporate the two minor changes proposed recently by Mulvihill et al. 14, 21 Given the use of Ar as the bath gas, the Glarborg et al mechanism was modified to use the Ar-specific lowpressure limit for NO + O (+M) \rightleftharpoons NO₂ (+M) from Yarwood et al²² instead of the $M = N_2$ expression from Tsang and Herron²³; Glarborg et al include both expressions as options but use the $M = N_2$ expression by default.

In general, the GRI 3.0 mechanism is under-reactive, predicting $\rm H_2O$ formation that is slower than the experimental data. The $\rm H_2O$ formation predicted by the Mathieu et al mechanism is generally a bit faster than that of GRI 3.0 but is still quite a bit slower than the data. The Zhang et al and Glarborg et al mechanisms do a fair job of predicting the experimental data except at the coldest temperatures for Mix 2 and Mix 3, where the predicted $\rm H_2O$ formation at the end of the experiment is $\sim 30\%$ and $\sim 80\%$ of the experimental value, respectively.

The general trends noted in the preceding paragraph are further illustrated in Figure 4, which shows the time required to reach half of the maximum H_2O value possible for the mixture in question (assuming that only one of the O atoms from the NO_2 is free to form H_2O) versus the inverse temperature. As was also evident in Figure 3, the Zhang et al and Glarborg et al mechanisms perform the best overall in Figure 4, performing particularly well in the fuel-lean case and at higher temperatures.

In the fuel-lean mixture (Mix 1), a small amount of absorption was observed immediately behind the reflected shock wave, and this absorption increased with increasing T_5 . The cause of this immediate baseline shift was not broadband emission entering the I_t detector, as such emission was found to be negligible even at the highest temperatures by performing tests with the laser turned off (furthermore, any such emission would actually create an apparent decrease in absorption rather than an increase). Instead, it was determined that the small amount of initial absorption was due to interfering absorption by another species. This interference was discovered by performing an offline laser test, in which the laser was tuned to 1388.104 nm to sit in a region of very low H₂O absorption in the valley between the relatively weak H2O transitions at 1388.086 and 1388.112 nm, according to HITRAN 2004.²⁴ The results of the offline laser test are shown in Figure 5 alongside an online test at similar conditions. The

^bMeasured using plateau H₂O method.

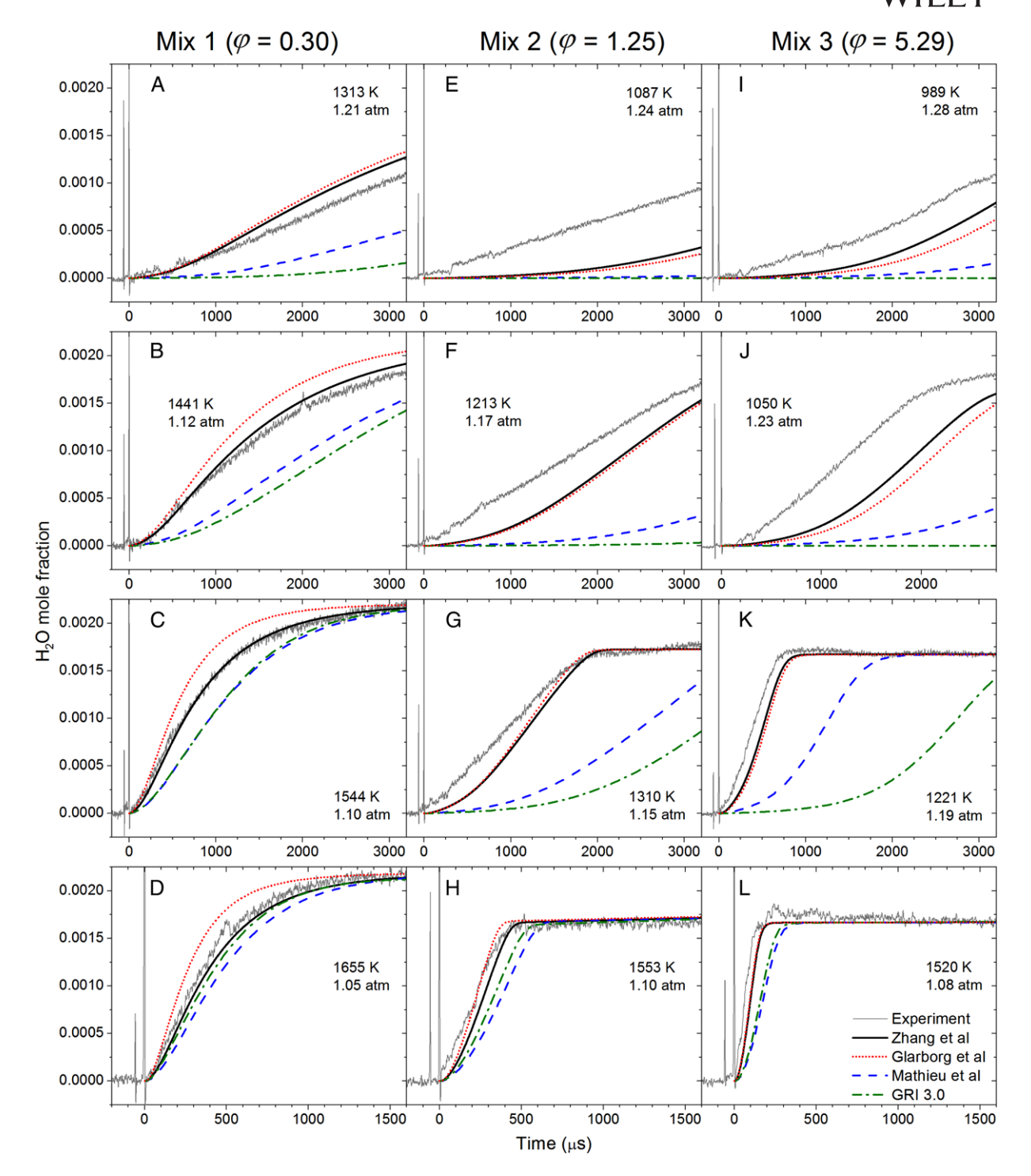


FIGURE 3 H₂O time histories measured in (A)-(D) Mix 1, (E)-(H) Mix 2, and (I)-(L) Mix 3 compared to the results of several chemical kinetics mechanisms. Thick solid lines: Zhang et al, ¹⁵ dashed lines: Mathieu et al, ¹⁷ dash-dot lines: GRI 3.0, ¹⁸ dotted lines: Glarborg et al. ¹⁹ The Mix 1 data have been slightly corrected for NO₂ interference (see text) [Color figure can be viewed at wileyonlinelibrary.com]

markedly different shapes of the absorption time histories from the online and offline tests strongly suggest that the initial absorption at time zero is due to some species other than $\rm H_2O$. To demonstrate the result of correcting for such interference, the offline absorption was subtracted from the online absorption to yield a corrected absorption time history, as

shown in Figure 5. The interference has a small effect at early times and becomes negligible at later times.

The most obvious candidate for the interfering species is NO₂ since it is present in the initial mixture and is also infrared-active, unlike H₂ and Ar. An additional test with a mixture of NO₂/Ar was performed, which yielded a nearly

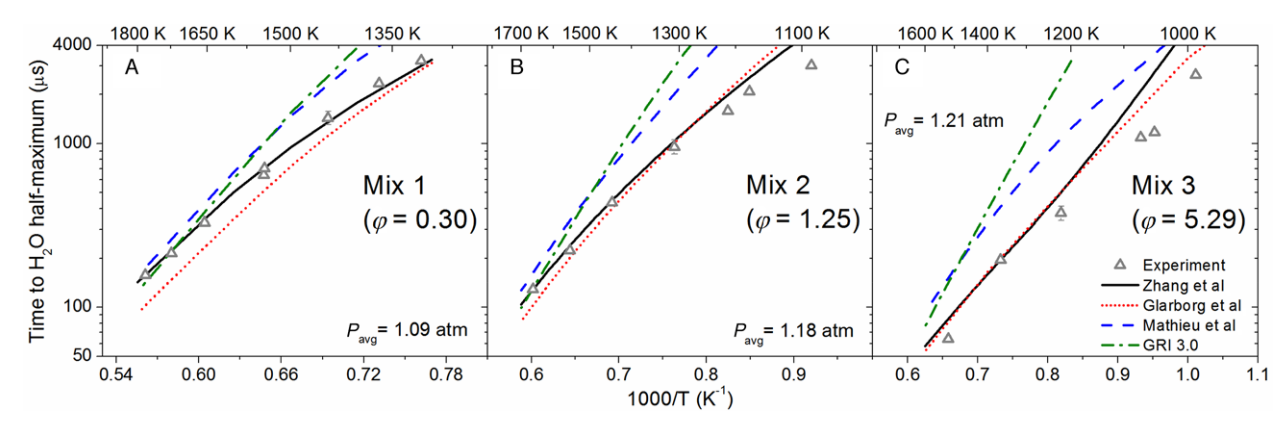


FIGURE 4 Arrhenius plot of the time to half the maximum possible H_2O for (A) Mix 1, (B) Mix 2, and (C) Mix 3. The estimated y-axis uncertainty is $\pm 10\%$. Thick solid lines: Zhang et al, ¹⁵ dashed lines: Mathieu et al, ¹⁷ dash-dot lines: GRI 3.0, ¹⁸ dotted lines: Glarborg et al. ¹⁹ The Mix 1 data have been slightly corrected for NO₂ interference (see text) [Color figure can be viewed at wileyonlinelibrary.com]

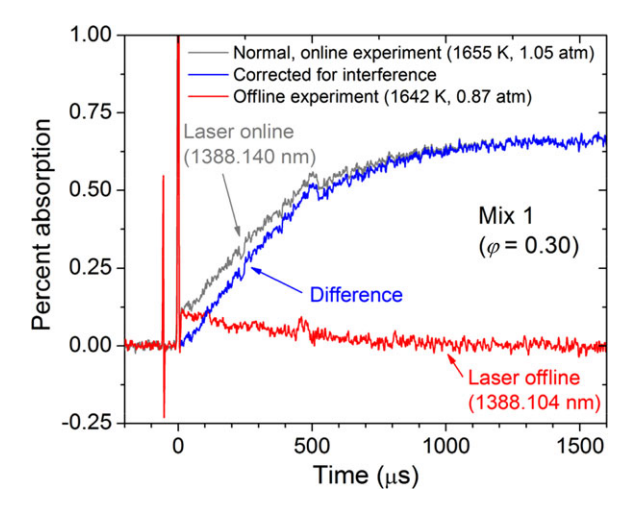


FIGURE 5 Offline and online laser tests in Mix 1 at similar conditions; the online test corresponds to the conditions of Figure 3(D). Also shown is the difference between the online and offline tests [Color figure can be viewed at wileyonlinelibrary.com]

identical shape to the offline test in Figure 5. Furthermore, the time history shapes from both offline tests matched closely the predicted shapes for NO₂ decay predicted by the Zhang et al mechanism (see Figure S10 for the NO₂/Ar experiment in the Supporting Information). These observations together confirmed that NO₂ was the interfering species. Interestingly, HITRAN 2004²⁴ does not predict any NO₂ absorption in this region. The nearly linear increase of the NO₂ absorption coefficient with temperature (see Figure S11 in the Supporting Information) suggests that this absorption may stem from a hot band of NO₂; HITRAN 2004 is designed for lower temperatures and, thus, has previously been found lacking in predictions of hot bands of CO₂.²⁵

In keeping with the conclusion that the interference was from NO_2 , the following method was used to make slight corrections to the data for Mix 1. The initial absorption at time zero was used to calculate an effective NO_2 absorp-

tion coefficient (Figure S11 in the Supporting Information). The NO₂ decay predicted by the Zhang et al mechanism was then used in conjunction with this effective absorption coefficient to subtract out the portion of the absorption time history corresponding to NO2 interference, with the balance being attributed to H₂O. This correction decreased with temperature; the experiment shown in both Figures 3(D) and 5 is the worst-case scenario for which the NO₂ correction is a maximum. The Mix 1 data shown in Figures 3 and 4 have been NO₂ corrected, whereas uncorrected Mix 1 data are provided in Figures S1 and S6-S9 in the Supporting Information. The NO₂ correction was not applied to Mix 2 or Mix 3, as no definitive signs of NO₂ interference at time zero were observed for these mixtures. This lack of interference was primarily due to the lower NO₂ content in these mixtures and also due to the lower temperatures at which these mixtures were tested.

4 | DISCUSSION

4.1 \mid H₂ oxidation by O₂ versus NO₂

For both the fuel-lean and fuel-rich cases, the presence of NO_2 supplies a stream of highly reactive radicals (primarily O atoms for the fuel-lean case and primarily H atoms for the fuel-rich case; see the reaction pathway analyses below). This source of radicals allows the H_2 - NO_2 system to bypass the induction period associated with H_2 - O_2 mixtures in which the radical pool (O, H, OH) grows to a suitable size to permit explosion. As an example of the difference between these two systems, Figure 6 shows H_2O profiles measured in the H_2 - NO_2 system (this study) and in the H_2 - O_2 system (from Mulvihill and Petersen²⁶). In contrast to the instantaneous H_2O formation observed in the H_2 - NO_2 mixture, the H_2 - O_2 mixture displays an induction delay time before the sharp increase in H_2O concentration. The comparison in Figure 6

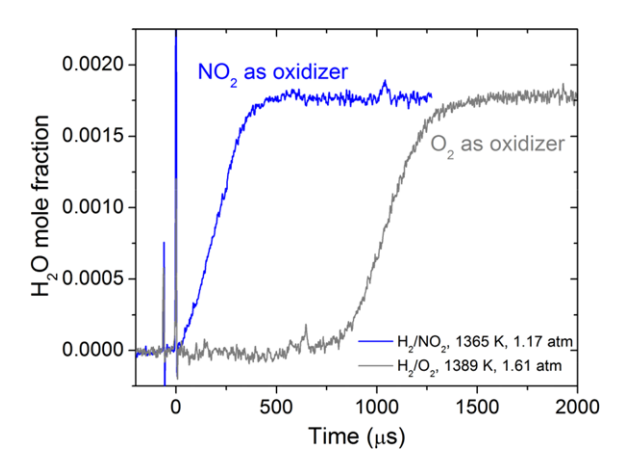


FIGURE 6 H₂O profiles measured in 0.168% NO₂/1.778% H₂/balance Ar (this work) and 0.1% O₂/0.9% H₂/balance Ar (from Mulvihill and Petersen²⁶). The H₂-O₂ results have been scaled by a factor of 0.89 for comparison [Color figure can be viewed at wileyonlinelibrary.com]

exemplifies the promoting effect that is generally associated with NOx additions to hydrocarbon mixtures.

4.2 | Reaction pathway analysis: Fuel-lean conditions

To explore the important routes of H_2O formation and the promoting effect of NO_2 , a reaction pathway analysis was performed using the Zhang et al mechanism at $\varphi=0.30$, 1441 K, 1.12 atm (the conditions of Figure 3(B)). This analysis revealed that during the first $\sim 50~\mu s$, NO_2 decomposition takes place primarily through the reaction

$$2NO_2 \leq NO_3 + NO.$$
 (R1)

Although the NO produced by (R1) can be viewed as a stable product at the timescales of the current experiments, the NO_3 is immediately recycled to NO_2 via

$$NO_3 (+M) \leftrightarrows NO_2 + O (+M)$$
. (R-2)

Thus, the sequence of (R1) and (R-2) ultimately produces one O atom and one NO molecule from one NO_2 molecule. NO_2 decomposition also takes place during the initial $\sim 5~\mu s$ due to

$$NO_2(+M) \leftrightarrows NO + O(+M),$$
 (R-3)

but this reaction rapidly becomes less important in favor of NO₂ consumption by the O atoms produced by (R-2) and, to a smaller extent, (R-3) through the reaction

$$NO_2 + O \leq NO + O_2$$
. (R4)

Note that (R-2) and (R-3) are written here in the backward direction relative to their notation in three mechanisms considered herein, save that GRI 3.0 does not contain (R-2).

NO2 is also attacked by H2 via

$$NO_2 + H_2 \leq HONO + H.$$
 (R5)

This channel is relatively minor (although not insignificant) in the fuel-lean mixture but is discussed in more detail for fuelrich conditions in the following section.

The O atoms formed by (R-2) and (R-3) are primarily consumed by (R4). However, a small portion of the O atoms (~10% during the initial ~20 μs) react with H_2 in the chain-branching reaction

$$H_2 + O \leftrightharpoons H + OH.$$
 (R6)

The role of (R6) is critical in two regards. First, it supplies OH radicals, which can react with H_2 via

$$H_2 + OH \leftrightharpoons H + H_2O,$$
 (R7)

which is the dominant pathway of H_2O formation in all three mixtures. The second role of (R6) is that it forms an H atom, which is then free to react with NO_2 :

$$NO_2 + H \leq NO + OH.$$
 (R8)

(R8) produces OH, which can then react via (R7) to form further H_2O and H, thereby establishing a catalytic cycle between (R7) and (R8).

The HO_2 radical also plays a noticeable role in $\mathrm{H}_2\text{-NO}_2$ chemistry. Throughout the entirety of the experimental timescales considered, HO_2 is produced almost exclusively via

$$NO_2 + OH \leftrightharpoons HO_2 + NO$$
 (R-9)

and proceeds to react with OH atoms via

$$HO_2 + OH \leftrightharpoons H_2O + O_2.$$
 (R10)

Although the sequence (R-9) and (R10) does ultimately produce H_2O , it does so by consuming two OH radicals and thus inhibits the overall reactivity of the mixture by competing with (R7) for OH. (R-9) is written here in the backward direction from its notation in the mechanisms.

4.3 | Reaction pathway analysis: Fuel-rich conditions

An additional reaction pathway analysis was conducted using the Zhang et al¹⁵ mechanism at $\varphi = 5.29$, 1050 K, 1.23 atm (the conditions of Figure 3(J)). Many of the key reactions for fuel-lean conditions were still found to play a role. However, (R5) becomes a much more significant pathway at fuel-rich

conditions partly due to increased H_2 concentration, accounting for $\sim 20\%$ of the NO_2 consumption of (R1) and providing a direct route for H-atom formation. These H atoms can then react with NO_2 via (R8) to strengthen the catalytic cycle between (R7) and (R8).

Another reaction between NO_2 and H_2 ,

$$NO_2 + H_2 \leftrightharpoons HNO_2 + H,$$
 (R11)

becomes more important at fuel-rich conditions, producing H atoms at $\sim 10\%$ of the rate of (R5). Furthermore, the HNO₂ formed by (R11) immediately isomerizes to HONO, and a portion of the HONO produced by (R5) and ultimately by (R11) can decompose via

$$HONO(+M) \leftrightharpoons OH + NO(+M)$$
 (R-12)

to further supply (R7) with OH radicals. (R-12) is written here in the backward direction from its notation in the mechanisms, save that GRI 3.0 does not contain (R-12).

Finally, the fuel-rich mixture (Mix 3) was tested at lower temperatures as it is more reactive than the fuel-lean mixture (Mix 1) due to the influence of (R5) and (R11). These lower temperatures generally cause the NO₂ consumption via (R1) and (R-2) to take place at a much slower rate, meaning that O atoms are generally less available and thus less critical to the overall reaction for fuel-rich conditions.

4.4 | H₂O sensitivity analysis

To investigate the differences between the four mechanisms under consideration, a comparative H_2O sensitivity analysis was conducted with all four mechanisms in all three mixtures, and the results for two of the mixtures are shown in Figure 7 A positive sensitivity for a reaction means that increasing its rate would accelerate H_2O formation, whereas a negative sensitivity means increasing the rate would slow H_2O formation. The results for Mix 2 are not shown but were generally intermediates of those for Mix 1 and Mix 3. The results of the Glarborg et al 19 mechanism are not shown in Figure 7 as they were nearly identical to those of the Zhang et al 15 mechanism.

Several key differences between the fuel-lean and fuel-rich cases discussed during the reaction pathway analysis can be observed in the sensitivity analysis of Figure 7 for the results using Zhang et al. For example, the reduced O-atom concentration at fuel-rich conditions causes a reduced sensitivity to (R6) relative to the fuel-lean case. Also, the NO₂ decomposition reaction (R-3) is negligible for both Zhang et al and Mathieu et al for fuel-rich conditions.

The reactions noted as absent from GRI 3.0 in Figure 7 explain a large part of the general inability of GRI 3.0 to accurately reproduce the experimental data. First, GRI 3.0 does not contain the species NO₃, meaning it is missing the key NO₂ decomposition pathway of (R1) and the subsequent

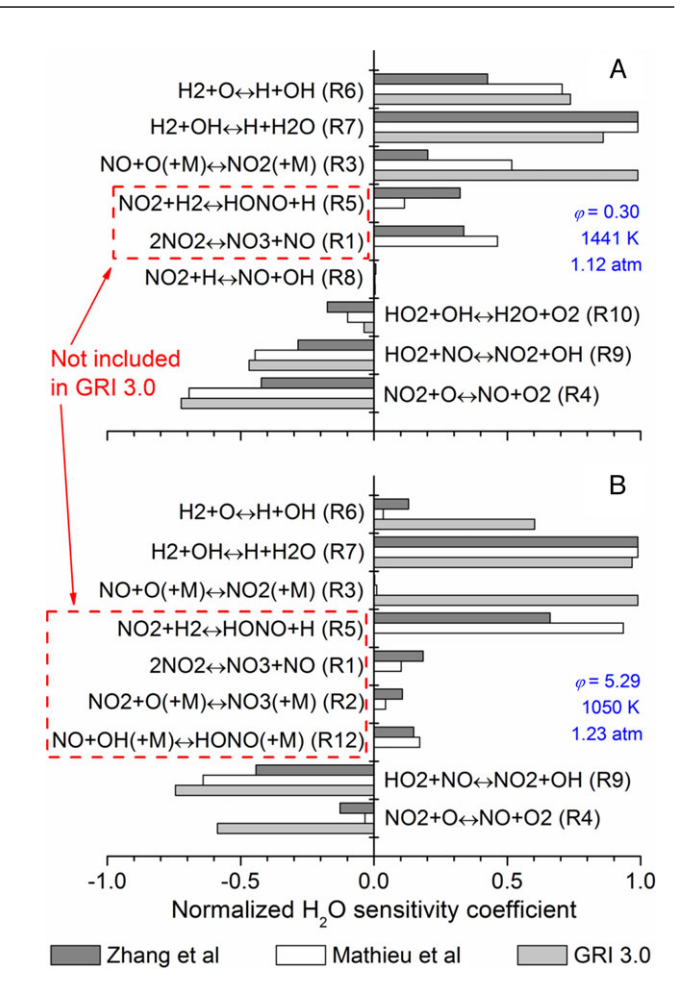


FIGURE 7 Normalized H_2O sensitivity coefficients at conditions corresponding to (A) Figure 3(B) and (B) Figure 3(J). Analysis was performed at 500 μ s after the reflected shock wave using Zhang et al, ¹⁵ Mathieu et al, ¹⁷ and GRI 3.0. ¹⁸ All reactions are written in the directions given in the mechanisms [Color figure can be viewed at wileyonlinelibrary.com]

O-producing reaction (R-2). This absence is particularly marked at fuel-lean conditions but also plays a role at fuel-rich conditions. Second, GRI 3.0 does not contain HONO, which plays a key role through the (R5) and (R11) pathways of H-atom production. The absence of these reactions and key species in GRI 3.0 leads to an overdependence on the NO₂ decomposition pathway (R-3), which is far too slow to reproduce the experimental data, particularly at lower temperatures. Of course, the inability of GRI 3.0 to reproduce these data is not particularly surprising given that GRI 3.0 was developed for more common systems (eg, natural gas in air), but the authors wish to highlight that GRI 3.0 should not be used for modeling of EGR applications.

The Mathieu et al mechanism generally outperforms GRI 3.0 (except for slight differences at the high-temperature end of the experiments) but is still noticeably less reactive than both the Zhang et al mechanism and the experimental data. Since the Mathieu et al mechanism contains all of the same

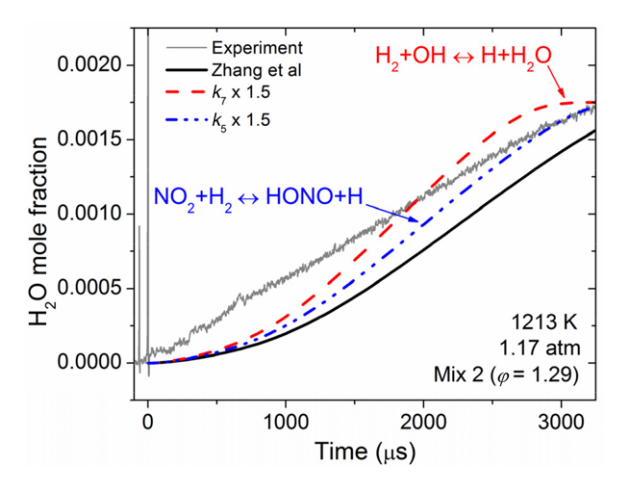


FIGURE 8 H₂O time history at the conditions of Figure 3(F) alongside model predictions from Zhang et al¹⁵ with variations in the rates of (R5) and (R7). Thick solid line: unmodified mechanism, dashed line: $k_7 \times 1.5$, dash-dot-dot line: $k_5 \times 1.5$ [Color figure can be viewed at wileyonlinelibrary.com]

key species outlined in the preceding paragraph as the Zhang et al mechanism, the differences between the two mechanisms arise from the reaction rates employed in each. For example, Zhang et al used a rate for (R1) from Tsang and Herron, 23 whereas Mathieu et al used the rate from Konnov. The Tsang and Herron rate is $\sim 60\%$ faster than the Konnov rate at the high-temperature end of this study (~ 1660 K) and over seven times faster at the low-temperature end (~ 915 K). The slower rate from Konnov partially explains the less-reactive nature of the Mathieu et al mechanism. Additionally, the rate for the (R5) used by Zhang et al is ~ 12 times faster than that used by Mathieu et al at the high-temperature end of this study and ~ 2.4 times faster at the low-temperature end, which further explains the differences between these two mechanisms.

4.5 | Initial H₂O formation

Evident in Figure 3 is the fact that at fuel-rich conditions (Mix 2 and Mix 3), the experimental data reveal a much faster rate of H₂O formation immediately after the reflected shock wave than do the model predictions, even for the two mechanisms that most accurately reproduced the experimental data. To investigate this early time discrepancy further, a sensitivity analysis was performed using the mechanism of Zhang et al at the conditions of Figure 3(F). This analysis revealed that the two dominant reactions at early times (< 100 µs) are (R5) and (R7). Zhang et al (as well as Glarborg et al) used k_5 from the theoretical work of Chai and Goldsmith, 28 who only provided an uncertainty estimate for their activation energy (±1.5 kcal/mol). An uncertainty factor of 1.5 was assumed for k_5 . An uncertainty factor of 1.5 for k_7 was taken from the review by Baulch et al.²⁹ Figure 8 shows the effects of independently varying k_5 and k_7 by these uncertainty factors. It can be seen that even with these changes, the initial predicted $\rm H_2O$ formation is still much slower than the experimental data; nearly identical results were obtained when performing the same analysis with the Glarborg et al mechanism. At this point, it remains unclear as to what could be causing the discrepancy observed in Figures 3 and 8, and further work, such as the possible addition of a new reaction pathway, is needed to address this issue.

5 | CONCLUSIONS

 $\rm H_2O$ time histories were obtained using a laser absorption technique in fuel-lean, near-stoichiometric, and fuel-rich mixtures of $\rm H_2\text{-}NO_2$. These data are the first shock-tube speciation data to be reported in the $\rm H_2\text{-}NO_2$ system. The predictions of four chemical kinetic mechanisms were compared to the data. The oldest mechanism (GRI 3.0) was found to poorly reproduce the data except at the highest temperatures, whereas the most recent mechanisms (Zhang et al and Glarborg et al) were found to reproduce the data fairly well. A detailed chemical kinetic analysis revealed that the inaccuracy of GRI 3.0 was largely due to the exclusion of reactions involving the species $\rm NO_3$ and $\rm HONO$.

The insights gained from these new data can ultimately be applied to practical conditions for gas turbines and other related applications. EGR applications involving high NOx concentrations in the recirculated gases should be modeled using a more recent chemical kinetic mechanism that fully accounts for the species present in the combustion process. Furthermore, even the mechanisms most successful at reproducing the new experimental data were still underreactive to varying degrees at nearly every condition, although the predictions for the fuel-lean mixture were quite accurate. Further refinement of these mechanisms is still required to improve the modeling of NOx-related chemistry for EGR and other applications. For example, the role of the reaction $NO_2 + H_2$ \leftrightarrows HONO + H (R5) was found to be quite critical, yet two of the more-recent mechanisms investigated in this work employ significantly different rates for this reaction. Finally, predicted H₂O profiles were found to differ significantly from the experimental data at colder temperatures and fuel-rich conditions. Variations of two key reactions were unable to rectify this discrepancy, highlighting the need for further refinement of H₂-NO2 chemistry.

ACKNOWLEDGMENTS

Support for this work was provided by the TEES Turbomachinery Laboratory and by the National Science Foundation, grant number CBET-1706825.

ORCID

Clayton R. Mulvihill (b) https://orcid.org/0000-0002-4256-1311

REFERENCES

- Caton JA. Thermodynamic considerations regarding the use of exhaust gas recirculation for conventional and high efficiency engines. J Eng Gas Turbines Power. 2017;139:092803.
- Chan YL, Barnes FJ, Bromly JH, Konnov AA, Zhang DK. The differentiated effect of NO and NO₂ in promoting methane oxidation. *Proc Combust Inst.* 2011;33:441-447.
- Olm C, Zsély IG, Pálvölgyi R, et al. Comparison of the performance of several recent hydrogen combustion mechanisms. Combust Flame. 2014;161:2219-2234.
- Mathieu O, Levacque A, Petersen EL. Effects of NO₂ addition on hydrogen ignition behind reflected shock waves. *Proc Combust Inst*. 2013;34:633-640.
- Mueller MA, Yetter RA, Dryer FL. Flow reactor studies and kinetic modeling of the H₂/O₂/NOx and CO/H₂O/O₂/NOx reactions. *Int J Chem Kinet*. 1999;31:705-724.
- Dayma G, Dagaut P. Effects of air contamination on the combustion of hydrogen—Effect of NO and NO₂ addition on hydrogen ignition and oxidation kinetics. *Combust Sci Technol*. 2006;178:1999-2024.
- Ashmore PG, Levitt BP. The thermal reaction between hydrogen and nitrogen dioxide. Part 2. Experimental work on the kinetics of the reaction. *Trans Faraday Soc.* 1956;52:835-848.
- Ashmore PG, Levitt BP. The thermal reaction between hydrogen and nitrogen dioxide. Part 3. Further experimental work on the kinetics: reaction mechanism. *Trans Faraday Soc.* 1957;53:945-954.
- Ashmore PG, Levitt BP. The thermal reaction between hydrogen and nitrogen dioxide. Part 4. Thermal ignitions of hydrogen and nitrogen dioxide. *Trans Faraday Soc.* 1958;54:390-393.
- 10. Rosser WA, Wise H. Kinetics of reaction between hydrogen and nitrogen dioxide. *J Chem Phys.* 1957;26:571-576.
- Sawyer RF, Glassman I. The reactions of hydrogen with nitrogen dioxide, oxygen, and mixtures of oxygen and nitric oxide. Symp (Int) Combust. 1969;12:469-479.
- Park J, Giles ND, Moore J, Lin MC. A comprehensive kinetic study of thermal reduction of NO₂ by H₂. J Phys Chem A. 1998;102:10099-10105.
- 13. Mueller MA, Gatto JL, Yetter RA, Dryer FL. Hydrogen/nitrogen dioxide kinetics: derived rate data for the reaction $H_2 + NO_2 = HONO + H$ at 833 K. *Combust Flame*. 2000;120:589-594.
- 14. Mulvihill CR, Mathieu O, Petersen EL. The unimportance of the reaction $H_2 + N_2O \leftrightharpoons H_2O + N_2$: a shock-tube study using H_2O time histories and ignition delay times. *Combust Flame*. 2018;196:478-486.
- Zhang Y, Mathieu O, Petersen EL, Bourque G, Curran HJ. Assessing the predictions of a NO_x kinetic mechanism on recent hydrogen and syngas experimental data. *Combust Flame*. 2017;182:122-141.
- 16. Schneider W, Moortgat GK, Tyndall GS, Burrows JP. Absorption cross-sections of NO_2 in the UV and visible region (200-700 nm) at 298 K. *J Photochem Photobiol*, A. 1987;40:195-217.

- 17. Mathieu O, Levacque A, Petersen EL. Effects of N₂O addition on the ignition of H₂-O₂ mixtures: experimental and detailed kinetic modeling study. *Int J Hydrogen Energy*. 2012;37:15393-15405.
- Smith GP, Golden DM, Frenklach M, et al. GRI-Mech 3.0. http://www.combustion.berkeley.edu/gri-mech/version30/text30. html. (accessed May 14, 2019).
- Glarborg P, Miller JA, Ruscic B, Klippenstein SJ. Modeling nitrogen chemistry in combustion. *Prog Energy Combust Sci.* 2018:67:31-68.
- Chaos M, Dryer FL. Chemical-kinetic modeling of ignition delay: considerations in interpreting shock tube data. *Int J Chem Kinet*. 2010;42:143-150.
- 21. Mulvihill CR, Mathieu O, Petersen EL. Corrigendum to "The unimportance of the reaction $H_2 + N_2O \leftrightarrows H_2O + N_2$: a shock-tube study using H_2O time histories and ignition delay times" [Combustion and Flame 196 (2018) 478-486]. *Combust Flame*. 2019;204:430.
- 22. Yarwood G, Sutherland JW, Wickramaaratchi MA, Klemm RB. Direct rate constant measurements for the reaction oxygen atom + nitric oxide + argon → nitrogen dioxide + argon at 300-1341 K. J Phys Chem. 1991;95:8771-8775.
- Tsang W, Herron JT. Chemical kinetic data base for propellant combustion I. Reactions involving NO, NO₂, HNO, HNO₂, HCN and N₂O. *J Phys Chem Ref Data*. 1991;20:609-663.
- Rothman LS, Jacquemart D, Barbe A, et al. The HITRAN 2004 molecular spectroscopic database. J Quant Spectrosc Radiat Transfer. 2005;96:139-204.
- Mulvihill CR, Petersen EL. High-temperature argon broadening of CO₂ near 2190 cm⁻¹ in a shock tube. Appl Phys B. 2017;123:255.
- Mulvihill CR, Petersen EL. Concerning shock-tube ignition delay times: an experimental investigation of impurities in the H₂/O₂ system and beyond. *Proc Combust Inst.* 2019;37:259-266.
- Konnov AA. Implementation of the NCN pathway of prompt-NO formation in the detailed reaction mechanism. *Combust Flame*. 2009;156:2093-2105.
- Chai J, Goldsmith CF. Rate coefficients for fuel+NO₂: predictive kinetics for HONO and HNO₂ formation. *Proc Combust Inst.* 2017;36:617-626.
- Baulch DL, Bowman CT, Cobos CJ, et al. Evaluated kinetic data for combustion modeling: supplement II. J Phys Chem Ref Data. 2005;34:757-1397.

SUPPORTING INFORMATION

Additional supporting information may be found online in the Supporting Information section at the end of the article.

How to cite this article: Mulvihill CR, Mathieu O, Petersen EL. H₂O time histories in the H₂-NO₂ system for validation of NOx hydrocarbon kinetics mechanisms. *Int J Chem Kinet*. 2019;51:669–678. https://doi.org/10.1002/kin.21286